Ecological Indicators 178 (2025) 113838

Contents lists available at ScienceDirect

Ecological Indicators

journal homepage: www.elsevier.com/locate/ecolind

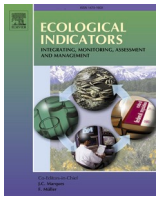

The global drought-sensitive areas will expand in the future

Qiaoqiao Li [a], Aizhong Ye [a,*], Reshmita Nath [b], Yuhang Zhang [a,c], Junju Zhou [d]

[a] State Key Laboratory of Earth Surface Processes and Disaster Risk Reduction, Faculty of Geographical Science, Beijing Normal University, Beijing 100875, China
[b] King Abdullah University of Science and Technology (KAUST), Thuwal, Saudi Arabia
[c] Department of Infrastructure Engineering, The University of Melbourne, Parkville 3010, Australia
[d] College of Geography and Environment Science, Northwest Normal University, Lanzhou 730070, China

ARTICLE INFO

Keywords:
Drought-sensitive areas
Future
Expand
Climate change
Global

ABSTRACT

Climate change and human activities are intensifying drought conditions, significantly altering drought propagation processes. However, these changes remain insufficiently understood, particularly for typical drought partitions such as humid, drought-sensitive, and arid types of drought propagation partition. Therefore, this study examines the change on these partitions under three Shared Socioeconomic Pathways (SSP1-2.6, SSP3-7.0, and SSP5-8.5) to elucidate global drought trends. The results show that the global drought-sensitive area will expand by 1.89×10^6 km^2, which is roughly the size of Sudan (1.88×10^6 km^2). Notably, in South America alone, the drought-sensitive area is projected to increase by 1.27×10^6 km^2, equivalent to the size of Niger. While in South America the humid partition will shrink by 1.45×10^6 km^2, with nearly 60 % transitioning into drought-sensitive areas. Overall, human activities are expected to drive drought partitions in an unfavorable direction, with approximately 3.26×10^6 km^2 will shift from humid-type partition to drought-sensitive areas or from drought-sensitive areas to arid-type partitions under the SSP5-8.5 scenario, similar to the size of India (3.29×10^6 km^2). Among all the climate zones, the changes are most notable in the humid and semi-arid regions. Significant transformations in drought propagation patterns are evident in the Great Plains of the United States of America, southern and central Europe, and the Amazon basin in South America, where declining precipitation and intensifying land–atmosphere coupling are the main driving factors. These findings provide critical insights for drought prediction and management in the context of climate change.

1. Introduction

Drought and flood disasters are among the most complex and severe natural hazards, which has profound impacts on socio-economies across the globe (Zheng, 2000; Mondal et al., 2023; Mishra & Singh, 2010). In the recent years, due the intensification of greenhouse warming and climate change, there is a widespread consensus among the scientific communities that the severity of drought conditions will worsen in future, accompanied by an increased likelihood of extreme dry spells, erratic precipitation, and extreme heat events, leading to faster onset of drought events (Yin et al., 2023; Zhou et al., 2023; Yuan et al., 2023). Observational data and climate model simulations indicate that global warming will accelerate drying of the arid regions, with a continued expansion of arid zones and a contraction of humid regions, a trend that is likely to persist in the future (Asadi et al., 2022; Feng & Fu, 2013; Dai et al., 2004). Therefore, in response to these challenges, it is imperative to conduct an in-depth research on the evolution and propagation mechanisms of the droughts. In the context of climate change this study is of utmost importance for improving the drought prediction, early warning systems, and risk mitigation strategies (Sun et al., 2025).

The American Meteorological Society classifies the drought into four types: meteorological drought, hydrological drought, agricultural drought, and socio-economic drought, where each category is corresponding to a specific type of moisture deficiency (Heim, 2002). Among them, meteorological drought is the primary cause of the other three drought types (Mishra et al., 2015; Mishra & Singh, 2010) depending on the timescales for which water deficiency persists following a dry event with below normal precipitation. Agricultural drought often follows the meteorological drought and they occur simultaneously, and their frequency and severity are expected to increase in the future (Novick et al., 2016). Hydrological drought serves as an intermediate stage in the occurrence of drought that directly influences the socio-economic drought. Therefore, understanding the process of meteorological drought propagating into other drought types is crucial for a deeper

* Corresponding author.
E-mail address: azye@bnu.edu.cn (A. Ye).

https://doi.org/10.1016/j.ecolind.2025.113838
Received 16 March 2025; Received in revised form 12 June 2025; Accepted 1 July 2025
Available online 5 July 2025

comprehension of drought occurrence and their development into other types.

Drought propagation refers to the process in which the footprint of drought, originating from the abnormal meteorological conditions propagates into the hydrological systems and disrupts the normal hydrological cycle (Van Loon, 2013). Currently, drought propagation has become a focal point of research, with significant progress is made to understand its characteristics and evolution process (Zhang et al., 2023; Schumacher et al., 2022; Zhou et al., 2019; Ahmadi & Moradkhani, 2019). Previous studies indicate that drought propagation characteristics in the hydrological system e.g. Aggregation, attenuation, lag, extension, and the process varies across different regions (Zhang et al., 2022; Huang et al., 2025; Apurv et al., 2017). Due to climate change and increasing human activities, the drought propagation process is expected to undergo significant changes, however these changes have not been fully understood (Wu et al., 2022). Research suggests that drought propagation will intensify in the future, thereby increasing the likelihood of drought occurrences, with more than half of the global watersheds are expected to experience a significant deterioration in the early stages of drought propagation (Wu et al., 2022). Furthermore, hydrological processes tend to respond more rapidly to the meteorological droughts, e.g. drought propagation in the Yangtze River Basin of China (Ma et al., 2023), India (Sadhwani and Eldho, 2024), and the Han River Basin of South Korea (Jehanzaib et al., 2023) indicate that the speed of drought propagation is accelerating under climate change.

Existing research on drought propagation has primarily focused on the timing of the drought propagation. However, during the evolution of the drought events, factors beyond the propagation time, such as drought intensity, duration, and severity are also important for assessing the severity of droughts. From the perspective of drought propagation characteristics, Li et al., 2022a,b, 2024) introduced the concept of drought partitions and identified three major types of drought propagation partitions: Humid (H-dp), Drought-sensitive (S-dp), and Arid type drought propagation partition (A-dp). The global-scale study revealed that the area of S-dp has been expanding in the historical periods and the concept of drought partitions provides a new perspective for explaining the drought propagation process. In the context of climate change and human activities, the drought propagation process is expected to undergo alterations, but to what extent (duration and intensity) these changes affects the propagation process remain unclear, which warrants further investigation to fully understood the mechanism. Therefore, to better comprehend the drought propagation process, it is necessary to explore the evolution of drought partitions from multiple perspectives, including the presence or absence of human activity and its potential influence through Shared Socioeconomic Pathways (SSPs) for future scenarios. Due to the fundamental differences among SSPs —such as greenhouse gas emissions, land use changes, and socioeconomic development—the simulation outputs vary in terms of initial assumptions and driving factors, posing challenges for cross-scenario comparisons. To minimize the impact of such inconsistencies on the interpretation of results, this study uniformly employed the Inter-Sectoral Impact Model Intercomparison Project (ISIMIP 3b) framework, ensuring that all climate scenarios share a consistent data source and identical model structures (Frieler et al., 2017; Lange, 2019). We selected low (SSP1-2.6), medium (SSP3-7.0), and high (SSP5-8.5) greenhouse gas emission pathways because SSP1-2.6 reflects a sustainable pathway with strong mitigation efforts; SSP3-7.0 indicates regional rivalry and limited climate action; and SSP5-8.5 assumes continued fossil fuel reliance with minimal mitigation. These three scenarios are widely used to capture a representative range of future climate trajectories.

This study utilizes the data from ISIMIP 3b to investigate the variations in the drought propagation process under different scenarios. The aim is to further clarify the changing trends in global drought conditions, with the goal of providing important perspectives for drought prediction and management in the context of climate change.

2. Data set and Methodology

2.1. Data Sets

Precipitation and soil moisture data are primarily sourced from the ISIMIP 3b and ECMWF Reanalysis 5th Generation Land (ERA5-Land) datasets. In the ISIMIP 3b data, the precipitation is obtained from the five general circulation models (GCMs)—IPSL-CM6A, MPI-ESM1, MRI-ESM2, UKESM1, and GFDL-ESM4. The soil moisture data is derived from the Water Global Assessment and Prognosis Model, Version 2 (WaterGAP2) and Hanasaki Global Hydrological Model (H08) based models under the five GCMs, yielding a total of 10 datasets for each of the variables. The duration of the analysis spans from 1929 to 2014 (historical period) under different scenarios (with and without human activity influence), while from 2015 to 2100 (future period) the analysis is performed under three Shared Socioeconomic Pathways (SSPs): SSP1-2.6, SSP3-7.0, and SSP5-8.5, with a spatial resolution of 0.5 degrees. Additionally, we employed the ERA5-Land precipitation and soil moisture data, covering the period 1950–2014, with a spatial resolution of 0.1 degrees to validate the model output results.

Watershed boundaries are defined using the third-level boundaries from the Hydro BASINS (https://www.hydrosheds.org/products/hydrobasins). The climate classification data is derived from The Global Aridity Index (Global-Aridity_ET0) datasets, which provide high-resolution (30 arc-seconds) global raster climate data during the period from 1970 to 2000. These datasets were produced by Antonio Trabucco and Robert Zomer (Trabucco and Zomer, 2009). It has classified the watersheds into five climate zones based on the index values e.g. Hyper Arid (<0.03), Arid (0.03–0.2), Semi-Arid (0.2–0.5), Dry Subhumid (0.5–0.65), and Humid (>0.65). Since some of the watersheds span across the multiple climate zones, we have carefully combined the climate zones into the watershed boundaries to study the state of each watersheds across different climate zones.

2.2. Standardized precipitation Index (SPI) and Standardized soil moisture Index (SSMI)

Meteorological drought is typically defined by precipitation deficits, while agricultural drought is characterized by soil moisture shortages (Mishra et al., 2015; Mishra and Singh, 2010). To quantify them, the Standardized Precipitation Index (SPI) is used for the meteorological drought, while the Standardized Soil Moisture Index (SSMI) is used for the agricultural drought. Both the indices are calculated using the SPI method, which involves the probability distribution and then applying a normal standardization to derive the SPI and SSMI based indices (Mc Kee et al., 1993; Husak et al., 2007; Zhu et al., 2021). It allows to quantify the drought conditions across different regions and time periods. The SPI and SSMI at various time scales provide insights into different drought and flood scenarios. In this study, the SPI is calculated for the cumulative periods ranging from 1 to 12-month time scale, while the SSMI is computed using 1-month of cumulative value, enabling an assessment of the impact of meteorological drought on agricultural drought both from the monthly and annual perspectives.

2.3. Drought propagation duration

Pearson Correlation Coefficient (PCC) is used to determine the drought propagation time between the meteorological and agricultural droughts, a method widely used in the scientific studies to assess the response times between different drought types (Ding et al., 2021; Han et al., 2019; Huang et al., 2015, 2017; Xu et al., 2021; Zhang et al., 2021). The Pearson correlation is calculated between the meteorological drought indices at various time scales (SPI-1, SPI-2, …, SPI-n) and the agricultural drought (SSMI-1) at 1-month time scale. The SPI accumulation period (n) corresponding to the maximum Pearson coefficient (Pmax) is identified as the propagation time (Tn) from the

meteorological to agricultural drought.

2.4. Drought propagation Index

The Drought Propagation Index is a quantitative parameter that represents the propagation of a specific drought characteristic during the drought propagation process. Drought Intensity Propagation Index (DIP) and Drought Duration Propagation Index (DDP) represent the propagation of drought intensity and drought duration, respectively, from meteorological drought to agricultural drought (Li et al., 2022). The indices are calculated based on the formulas below:

$$DIP = \frac{SI_{SSMI1-Ln}}{MI_{SPIn-Ln}} (MI \neq 0) \quad (1)$$

$$DDP = \frac{SD_{SSMI1-Ln}}{MD_{SPIn-Ln}} (MD \neq 0) \quad (2)$$

In the formula, n represents the drought propagation time from meteorological drought to agricultural drought. The sequence length of the SPIn and SSMI1 are the same in terms of the number of months, represented by Ln. $MI_{SPIn-Ln}$ and $SI_{SSMIn-Ln}$ represent the average values of the drought sequences for SPI and SSMI, respectively, while $MD_{SPIn-Ln}$ and $SD_{SSMIn-Ln}$ represent the total drought duration for the corresponding SPI and SSMI drought sequences. The classification levels of the Drought Propagation Index are as follows Table 1.

2.5. Drought propagation partitions

Based on the classification of DIP and DDP, the global drought propagation partitions are divided into nine regions. The specific classification is shown in Table 2.

We focus on three primary propagation partitions: Humid type of drought propagation partition (H-dp), Drought-sensitive type of drought propagation partition (S-dp), and Arid type of drought propagation partition (A-dp). These three partitions cover the largest areas and are key regions for the propagation of meteorological drought to agricultural drought (Li et al., 2022, 2024).

To improve the accuracy of the Drought Propagation Index, a calibration process was conducted using the ERA5-Land data to adjust the DIP and DDP results derived from the ISIMIP data, with the calibration period spanning from 1950 to 2014. The process was carried out in several steps:

First, the DIP and DDP indices were calculated for each of the 10 ISIMIP datasets and one ERA5 dataset using a 30-year sliding window, resulting in 36 observations per dataset for each of the grid points. ERA5-Land data were then used to calibrate the ISIMIP datasets on a grid-by-grid basis. Seven calibration techniques were employed in this study: Random Forest (RF), Multi-layer Perceptron Regressor (MLPR), Support Vector Regressor (SVR), Linear Regression (LR), Polynomial Regression (PR), Ratio Correction Method, and Mean Bias Correction Method. The calibration accuracy was assessed by comparing the corrected ISIMIP data with the ERA5 data to see how well they matched the same drought partition classifications, as presented in Table 3. The results revealed that all of the seven methods yielded a calibration accuracy that exceeds 70 %. However, when examining the performance of the DIP at different time periods, it was found that the first five methods tend to overfit at longer time scales, while the Ratio and Mean Bias correction methods maintained the same trend characteristics as of the ISIMIP data. Based on the sensitivity analysis, the Mean Bias Correction Method was selected as the primary calibration approach and the 10 ISIMIP datasets were then adjusted using this method prior to the analysis.

Table 1
Classification of drought propagation index.

DIP or DDP	Index range
(0,0.9)	Weak (w)
[0.9,1.1)	Peer-to-peer (p-p)
(1.1, +∞)	Strong (s)

Table 2
Classification of Global Drought Partitions.

DDP DIP	Strong	Peer-to-peer	Weak
Weak	Arid I	IV	VII
Peer-to-peer	II	P-P V	VIII
Strong	III	VI	Humid IX

Table 3
Proportion of corrected ISIMIP data in the same drought partition as ERA5 data.

	RF	MLPR	SVR	LR	PR	Ratio	Bias
DDP	0.85	0.80	0.85	0.86	0.86	0.78	0.78
DIP	0.80	0.75	0.79	0.81	0.81	0.70	0.72

The following formula was used for correction:

$$Bias = \frac{1}{n} \sum_{i=1}^{n} (y_i - x_i) \quad (3)$$

x_i represents the DIP or DDP of the ISIMIP dataset during the calibration period, while y_i represents the DIP or DDP of the ERA5 dataset during the calibration period. N represents the number of samples during the calibration period, which is 36 in this case

$$y_{corr} = x_i + Bias \quad (4)$$

y_{corr} represents the corrected DIP or DDP result calculated from the ISIMIP data. x_i represents the DIP or DDP calculated from the ISIMIP data.

3. Results

3.1. Spatiotemporal distribution of drought propagation partitions across different periods

As shown in Fig. 1a, across all time periods the S-dp occupies the largest proportion globally, accounting for over 44 %. This is followed by the A-dp and H-dp, both of which account for over 19 %. The distribution of drought partitions shows high consistency at different climate zones (Fig. 1b): The A-dp is predominantly found in the Arid climate regions, H-dp is mainly distributed in the Humid regions, while S-dp is primarily distributedd in the transition zones between these two climate types. The distribution across continents is not uniform. In Africa and Australia, the A-dp and II-type drought partitions are predominant in the majority of the land masses, mostly concentrated in the desert regions. These areas are characterized by a longer duration of agricultural drought compared to the meteorological drought, with the intensity of the agricultural drought being lower than that of the meteorological drought. In the other continents, the S-dp occupies the largest proportion, followed by A-dp and H-dp types of partitions. In all the time scales, the combined proportion of A-dp, S-dp, and H-dp consistently exceeds 82 %, making them the primary type of drought partitions. Therefore, the focus of the following analysis will be on the three typical drought propagation partitions: A-dp, S-dp, and H-dp.

Here, we define the progression from the H-dp to S-dp to A-dp as a shift toward worsening conditions. In scenarios that are without human activity, the H-dp occupies the largest proportion globally, while the A-dp is the smallest. However, in future periods, from the SSP1-2.6 to the SSP5-8.5 scenario, the proportion of H-dp decreases gradually, while the proportion of S-dp and A-dp increases. This indicates that human activity drives the progression of drought partitions towards worsening

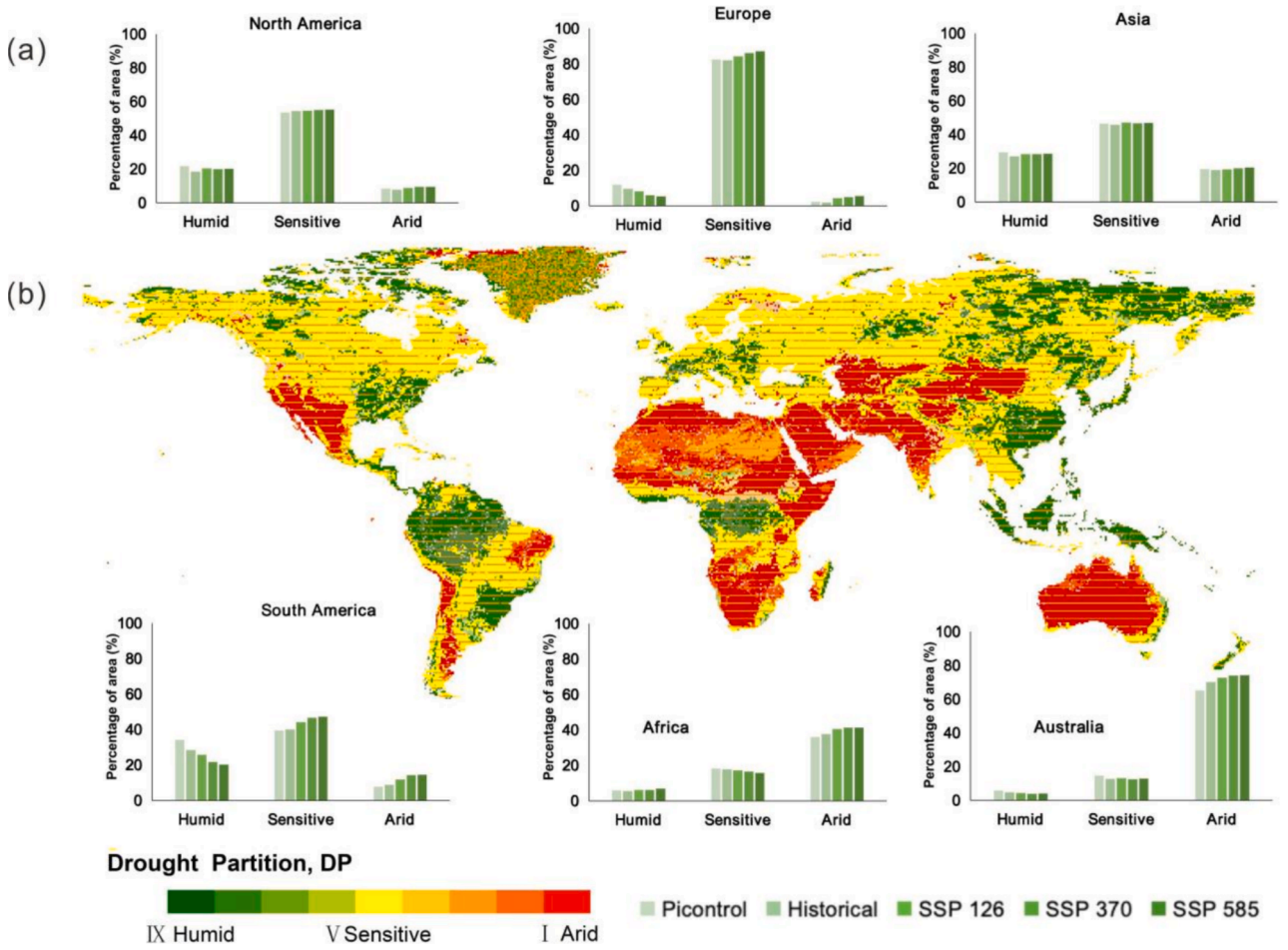

Fig. 1. a. Spatial distribution of drought partitions in the historical period; **b**. Spatial distribution of major drought partitions across continents (Humid (H-dp), Drought-sensitive (S-dp), and Arid type drought propagation partition (A-dp)). The striped areas indicate regions where the consistency of the 10 ISIMIP datasets reaches 70%.

conditions, with the extent of this progression growing from the SSP1-2.6 to the SSP5-8.5 scenario. The global S-dp will expand by 1.89 × 10^6 km^2, which is roughly the size of Sudan (1.88 × 10^6 km^2).

The degree of change varies across the continents e.g. the condition is worst in South America, the S-dp is projected to increase by 1.27 × 10^6 km^2, equivalent to the size of Niger, with the proportion of H-dp decreasing from 28.4 % in the historical period to 20.3 % under the SSP5-8.5 development scenario, nearly a third of the H-dp disappears. and the proportion of A-dp increases from 8.8 % to 14.7 %, effectively doubling the increase in future scenario. Europe follows the next, with a smaller proportion of A-dp and H-dp that corresponds nearly half of the Humid region disappears, and the area of Arid regions increases 3-fold in future.

3.2. Changes in drought partitions

3.2.1. Comparison with and without human activities

As shown in Fig. 2a, the largest proportion of global landmasses corresponds to the regions where each drought partition remains unchanged (H-dp remain H-dp, S-dp remain S-dp, A-dp remain A-dp). Meanwhile, as the scenario progresses from SSP1-2.6 to SSP5-8.5 in the future, the area where S-dp and H-dp remain unchanged decreases gradually, while the area where A-dp remains unchanged increases significantly. In the transition regions, the proportion of the area transitioning from S-dp to A-dp (S-A) and from H-dp to S-dp (H-S) is relatively large, indicating that the future development will worsen the drought partition conditions. As the development levels increase, the degree of the change towards aridity intensifies. Therefore, in our current analysis we focus on studying the regions that will experience more adverse condition in future. We represent the changes using the net growth in drought partitions and the calculation method is as follows: the net increase from H-dp to S-dp is the area transitioning from H-dp to S-dp minus the area transitioning from S-dp to H-dp. Similarly, the net increase from S-dp to A-dp is the area transitioning from S-dp to A-dp minus the area transitioning from A-dp to S-dp. The total net increase in the adverse direction is the sum of the two previous values.

Next, we compare the changes in drought partitions at different climate zones during historical periods, both for human activity and for without human activity influence (Fig. 2b). We find that, overall, human activities tend to worsen the drought partition (about 1 % of the area), particularly in regions with poor moisture conditions. We observe that the areas that are H-dp under the no human activity scenario and S-dp under the human activity scenario (H-S) have the largest proportion in the humid regions. In contrast, the areas that are S-dp under the no human activity scenario and A-dp under the human activity scenario (S-A) has the largest proportion in the semi-arid regions. The highest proportions are observed in Australia and South America (Fig. 2c, d). In regions with relatively favorable moisture conditions (Dry sub-humid regions and Humid regions), moderate human activity is beneficial for the region's development towards a positive direction, promoting a transition from A-dp to S-dp.

Finally, we delineate the specific regions by combining the climate and basin boundaries where human activities have the most severe negative impacts on drought partition conditions (Fig. 2e). These

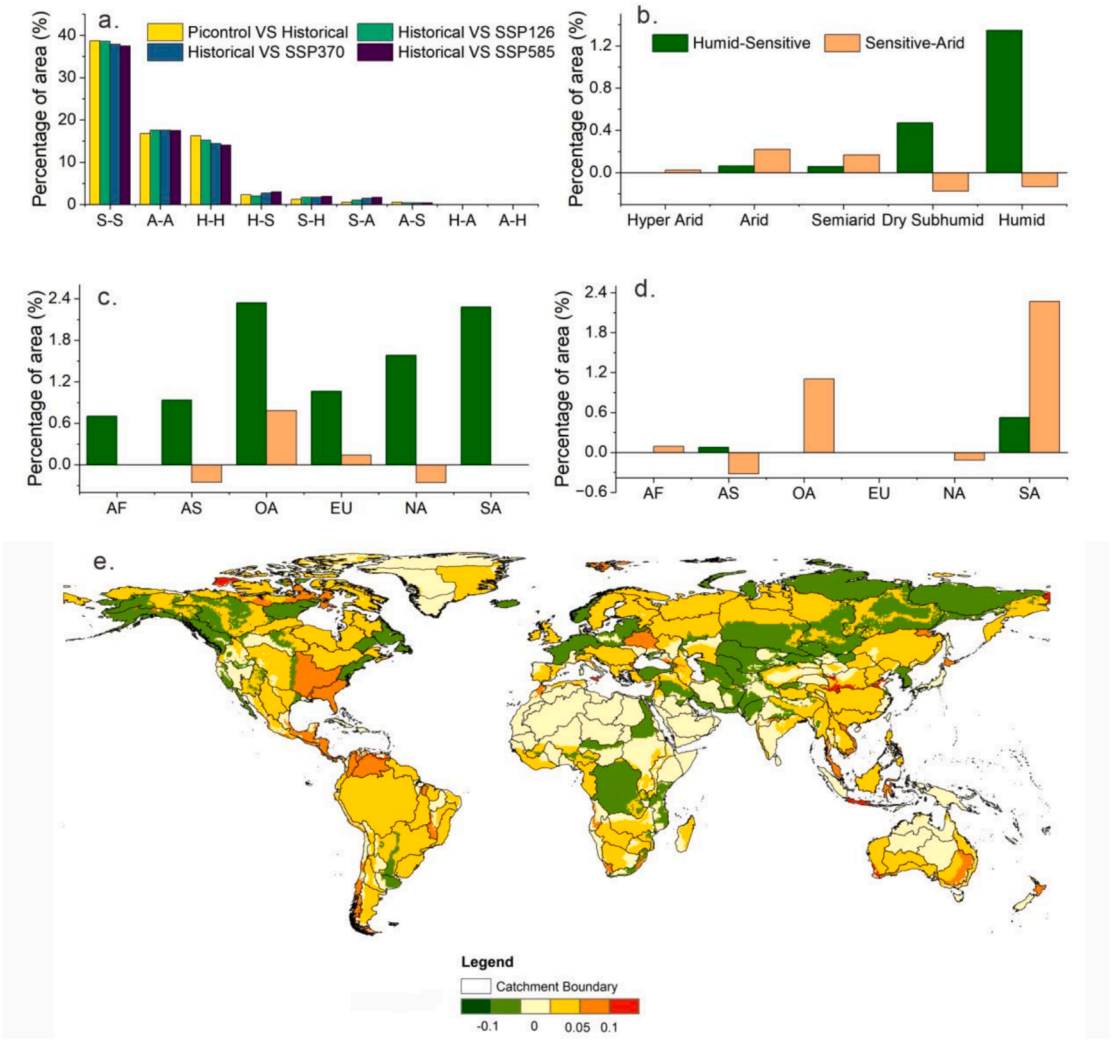

Fig. 2. Percentage of Area (%). a. The proportion of area change in global historical and future key drought partitions: S: Drought-sensitive, H: Humid type, A: Arid type, Picontrol: Scenario without human activity influence, Historical: Scenario with human activity influence. **b.** The net increase in the proportion of H-dp to S-dp (H-S) and S-dp to A-dp (S-A) under historical periods with and without human activity across each climate zone. **c.** The proportion of H-S and S-A in the humid regions of each continent (AF: Africa, NA: North America, AS: Asia, SA: South America, EU: Europe, OA: Oceania). **d.** The proportion of H-S and S-A in the arid regions of each continent. **e.** The proportion of net negative growth in drought propagation zones at the boundary of climate and basin.

regions are mainly located in the humid areas of the Mississippi River basin in North America, the Orinoco (9.7 %) and Magdalena (9.3 %) basins in northern part of South America, the Danube basin in Europe, and the Murray-Darling River basin in Australia (accounting for 5.7 % of the basin area). The regions where human activities have a positive impact are distributed in the Congo Basin and the humid regions in the high latitudes (Appendix 1b).

3.2.2. *Comparison of different future scenarios*

Globally, as the scenario progresses from SSP1-2.6 to SSP5-8.5, the extent of deterioration in drought partitions increases significantly. Under the SSP1-2.6, SSP3-7.0, and SSP5-8.5 scenarios, the proportion of the regions that are experiencing a net deterioration in the drought partitions increases by 1 %, 2 %, and 2.4 %, respectively. This means that approximately 3.26×10^6 km^2 will shift from H-dp to S-dp or from S-dp to A-dp under the SSP5-8.5 scenario.

In different climate zones, the regions with relatively favorable moisture conditions are evolving towards more severe conditions, particularly in the Humid and Semi-Arid regions. In contrast, the changes in the Hyper-Arid and Arid regions are less pronounced (Fig. 3a, b). In the Humid regions, the dominant transition is from H-dp to S-dp (Fig. 3a), while in the Semi-Arid regions, on one hand, there is a development towards H-dp from S-dp. On the other hand, the proportion of areas transitioning from S-dp to A-dp are also significant (Fig. 3b), with all continents showing a transition from S-dp to A-dp transitions in the Semi-Arid regions (Fig. 3e). The behavior varies within the same watershed area depending on different climate zones (Fig. 3f). For example, in terms of the H-dp to S-dp transition, the Mississippi River shows a clear trend of deterioration in the humid regions, while demonstrating a noticeable improvement in the Semi-Arid regions (Appendix 2). Regarding the S-dp to A-dp transition, the Murray-Darling Basin in Australia exhibits a clear trend of deterioration in the Semi-Arid regions, but an improvement in the Arid regions (Appendices 2).

Specifically, the extent of deterioration varies across the continents (Fig. 3f) e.g. South America, Europe, and North America are predominantly characterized by a transition from H-dp to S-dp. The most severely affected continent is South America, where the proportion of net deterioration is 2.8 %, 6.4 %, and 7.7 % under SSP1-2.6, SSP3-7.0 and SSP5-8.5, respectively. Notably, significant changes are observed in the humid regions of the Magdalena River, Guyana, Suriname, and the Cayenne-Humid regions, as well as in the San Francisco River Basin. Additionally, the large areas of the Amazon Basin exhibit a transition from H-dp to S-dp in the humid regions, accounting for 10 % of the total global area undergoing the conversion, although the proportion is

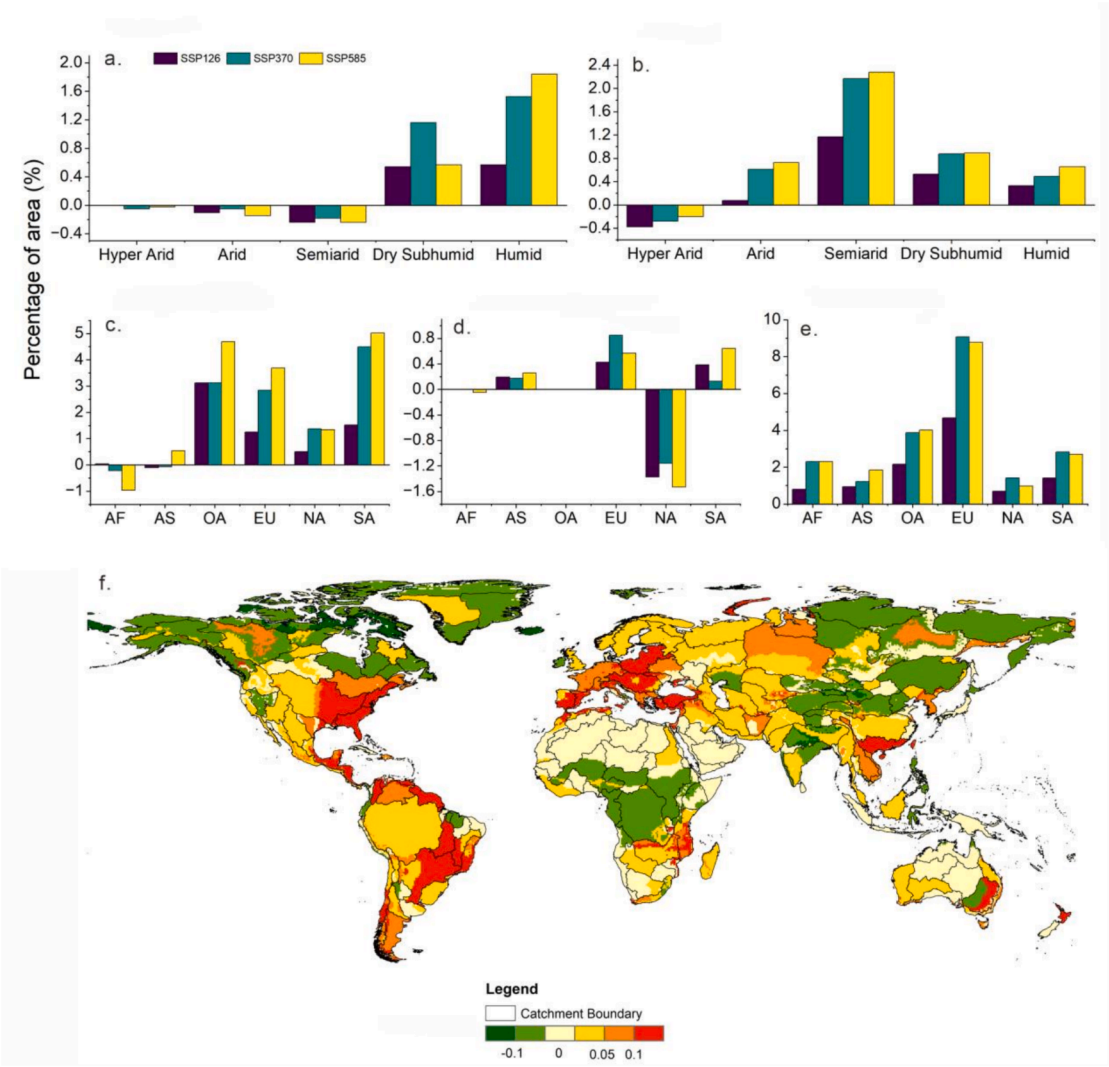

Fig. 3. Changes in drought zones under different future scenarios (SSP1-2.6, SSP3-7.0, SSP5-8.5). a. Proportion of net area in each climate zone where H-dp transitions to S-dp (H-S); **b.** Proportion of net area in each climate zone where S-dp transitions to A-dp (S-A); **c.** Proportion of H-S area in Humid regions of each continent; **d.** Proportion of H-S area in Semi-Arid regions of each continent; **e.** Proportion of S-A area in Semi-Arid regions of each continent; **f.** Proportion of net area in drought propagation partitions with negative growth, using climate and watershed boundaries (SSP5-8.5).

relatively small due to the vast size of the entire basin.

Next is the Europe, where the proportion of net deterioration is 2.7 %, 5.2 %, and 6.2 % under SSP1-2.6, SSP3-7.0 and SSP5-8.5, respectively. In Europe, all the basins, except for those in the far northern high-latitudes, are trending towards a deterioration. The most severe cases are found in the Semi-Arid regions of the Iberian Peninsula (37 % under SSP5-8.5) and the humid regions of the Danube Basin (24 % under SSP5-8.5). Notably, the direction of transition differs between these regions: the Iberian Peninsula is primarily undergoing a transition from S-dp to A-dp, while the Danube Basin is predominantly experiencing a transition from H-dp to S-dp.

In North America, the proportion of net deterioration is −0.12 %, 1.2 %, and 0.77 % under SSP1-2.6, SSP3-7.0 and SSP5-8.5, respectively. The most severe case is found in the humid regions of the Mississippi Basin in the Central Great Plains (23 % under SSP5-8.5). In Asia, the predominant transition is from S-dp to A-dp, where the proportion of net deterioration is 0.6 %, 1.1 %, and 1.9 % under SSP1-2.6, SSP3-7.0 and SSP5-8.5, respectively. The most severely affected basins are the Pearl River Basin in South East Asia (13.2 % under SSP5-8.5) and the Mekong River Basin (9 % under SSP5-8.5). In Central Asia and Western Asia, the primary transition is from S-dp to A-dp, while in Northern Asia, East Asia, and Southeast Asia the main transition is from H-dp to S-dp. Furthermore, in the Northern part of East Asian grassland areas and the Indian subcontinent, drought partitions are improving significantly. Notably, in the Amur River Basin (3.8 % under SSP5-8.5) the predominant transitions are from S-dp to H-dp, while in the Brahmaputra-Ganges Basin (3.5 % under SSP5-8.5) the primarily transitions are from A-dp to S-dp.

In Australia and Africa, the areas of humid regions are small, with only transitions from S-dp to A-dp are observed. In Australia, the proportion of net deterioration under different scenarios is 0.98 %, 1.69 %), and 1.49 % under SSP1-2.6, SSP3-7.0 and SSP5-8.5, respectively. The most affected region is the Murray-Darling Basin in the Semi-Arid region (11 % under SSP5-8.5) of Australia. In Africa, the proportion of net deterioration under different scenarios is 0.77 %, 1.2 %, and 1 % under SSP1-2.6, SSP3-7.0 and SSP5-8.5, respectively. These changes are primarily concentrated in the Semi-Humid regions of the Zambezi Basin in Southern Africa (11.4 % under SSP5-8.5), with transitions from S-dp to A-dp. Additionally, the areas surrounding the Congo Basin in the humid regions are showing some improvements.

4. Discussion

4.1. Identification of Hotspot regions of drought propagation transitions

The above results suggest that global drought partitions are transitioning towards an unfavorable direction, primarily manifested by the transition from H-dp to S-dp and then to A-dp. Numerous studies have shown that due to global warming, the degree of global aridification is intensifying, and the fractions of the arid areas are increasing continuously. Semi-arid regions are experiencing a significant warming intensification, which, through a warm-dry positive feedback mechanism has exacerbated the drying trend in the recent years. Dry sub-humid regions are transforming rapidly into semi-arid areas, and the extent of semi-arid regions is expanding continuously, resulting in a progressively more severe global aridification (Liu et al., 2023; Guan et al., 2018; Huang et al., 2016; Feng and Fu, 2013). This conclusion is highly consistent with our research findings.

The degree of changes in drought partitions varies across different regions. Based on the results above, the areas are severely affected by the unfavorable development of drought partitions include the Mississippi River basin in central and southern North America, the Amazon Basin in northern South America, the Iberian Peninsula and Danube in Europe, the Mekong and Pearl River basins in Asia, and the Murray-Darling River basin in Australia. Therefore, we pay special attention to the changes in drought conditions of these regions (Fig. 4).

4.2. Climatic drivers of drought propagation dynamics

Climate change is the direct cause of changes in the drought propagation process. The mechanism of meteorological drought propagation to the agricultural drought is complex, which resembles the feedback process that links soil moisture and precipitation. Precipitation directly contributes to an increase in soil moisture; while its deficit contributes to the soil drying in the dry periods (Cheng et al., 2015). On one hand, increased soil moisture promotes evapotranspiration and provides water vapor (Brubaker et al., 1993), while on the other hand, soil moisture influences precipitation by altering the redistribution of surface available energy between sensible and latent heat fluxes through dynamic feedback processes (Zhang et al., 2016). In most regions, precipitation decreases across all the future scenarios, especially in the Amazon Basin in South America and its surrounding areas, southern Europe, southern Africa, and southern Australia, where a significant reduction in precipitation is observed (Appendix 3). Correspondingly, soil moisture will also undergo significant changes in the future, with noticeable reductions in soil moisture has been observed in the regions mentioned above, At the same time, in all the regions where soil moisture increases, precipitation exhibits an identical increase and thereby establishing an implicit relationship between the two variables. (Appendix 4).Furthermore, for the Mississippi and Danube River basins, although precipitation has increased, soil moisture has decreased significantly, and there is a clear trend of drought partitions transitioning from H-dp to S-dp. This perhaps is related to the substantial increase in evapotranspiration in these regions (Liu et al., 2020; Konapala et al., 2020), where evaporation offsets the impact of increased precipitation on soil moisture. Meanwhile, in the future, land–atmosphere coupling will intensify in most of the regions globally, especially in North America and Europe. In the northern summer, model consensus indicates that the coupling between soil moisture and surface fluxes in the southern Great Plains of North America will be the strongest and is expected to increase further in future (Dirmeyer et al., 2013). At the same time, in the future, Central and Eastern Europe will exhibit stronger land–atmosphere coupling. (Seneviratne et al., 2006). The intense land–atmosphere coupling in these regions drives the shift from H-dp to S-dp.

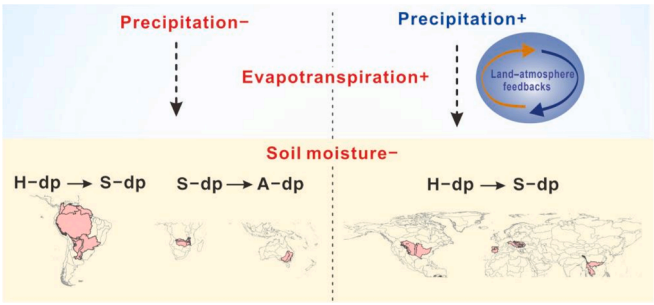

Fig. 4. Hotspot areas of unfavorable shifts in Drought Propagation Partitions.

4.3. Impacts of anthropogenic activities on drought propagation

In addition to climate change, we observe that human activities also play a significant role in the changes in drought propagation. While human activities may drive drought partitions in a positive direction, overall, they tend to exacerbate the negative progression of the drought partitions. From the SSP1-2.6 to the SSP5-8.5 scenario, the trends of drought partitions are worsening. Studies have shown that land management, water management and so on, can offset the wetting effects caused by the climate change, while human activities may further amplify the droughts induced by the climate change (Pokhrel et al., 2021) and soil moisture drying (Gu et al., 2019). The regions that are most severely affected by these changes are primarily located in the areas with strong human activities.

A typical example is the Amazon Basin, where large-scale deforestation has substantially modified regional climate conditions, leading to enhanced warming and drying trends. Among all continents, deforestation in the Amazon has the strongest climatic impact (Li et al., 2022; Kooperman et al., 2018; Mahmood et al., 2014). It alters surface biophysical properties (Bonan, 2008; Davin, 2010; Li et al., 2015) and amplifies regional responses to climate change (Li et al., 2022; Kooperman et al., 2018; Mahmood et al., 2014), thereby accelerating the shift in drought partitions (Lawrence and Vandecar, 2015; Costa and Foley, 2000; Zhang et al., 1996; Smith et al., 2023). Similarly, Europe has experienced severe soil moisture deficits (Rousi et al., 2022; Seneviratne et al., 2010; Miralles et al., 2014; Vogel et al., 2017), which may also contribute to the unfavorable transition of drought partitions in the region.

In some regions, however, human interventions may lead to more favorable developments in drought partitions. Taking China's Pearl River Basin as an example, future projections indicate a significant shift toward unfavorable drought partitions, with a large proportion of areas originally classified as H-dp expected to transition into S-dp. This shift suggests a weakening of the basin's natural buffering capacity against meteorological drought, which may be attributed to climate variability and land use changes. Nevertheless, it is worth noting that the Pearl River Basin has been a key region for ecological restoration and integrated watershed management in recent years. Initiatives such as the "Ecological Protection and High-Quality Development of the Pearl River Basin" and the implementation of the River Chief System have significantly enhanced ecological governance through strengthened water resource regulation, forest conservation, and pollution control. Existing studies have shown that wetland restoration, vegetation rehabilitation, and land use optimization have substantially improved ecosystem resilience in parts of the basin (Zhang et al., 2021; Li et al., 2019). Although the region is projected to undergo an unfavorable shift in drought partitions, incorporating these ecological restoration achievements into future assessments will help improve our understanding of the evolving regional drought risk. Moreover, continued ecological investment holds promise for mitigating or even reversing the unfavorable trajectory of drought propagation in the Pearl River Basin and potentially in other vulnerable regions.The regions that are most severely affected by these changes are primarily located in the areas with strong human activities.

4.4. Limitations and future research directions

In terms of data, although this study employed the multi-model, bias-corrected climate datasets provided by ISIMIP3b to analyze drought propagation characteristics—datasets widely recognized for their consistency and international credibility—some uncertainties and limitations remain. On the one hand, the spatial resolution of global climate model outputs (typically 0.5°) may be too coarse to fully capture topographic complexity or small-scale climatic variability in certain regions, potentially leading to biases in identifying drought-sensitive areas. On the other hand, despite being driven by the same input data and scenario settings, different models vary in their representations of physical processes, particularly precipitation simulation. Such structural differences can result in significant discrepancies in the projected spatial extent and intensity of drought propagation under future scenarios. To better illustrate the influence of model uncertainty, we present results from individual climate models in the supplementary materials (Appendices 5 and 6), highlighting both consistencies and divergences in drought-sensitive area identification across models.

It is worth noting that future research could consider integrating remote sensing data with ground-based observations and climate model outputs to enhance the spatial accuracy and process interpretability of drought propagation identification, especially in regions where in-situ monitoring is limited.

To mitigate the uncertainties described above, ERA5-Land data were used to bias-correct the ISIMIP simulations, and the analysis focused on relative changes in drought propagation trends rather than absolute values of drought indices. Additionally, a catchment-based spatial framework was adopted instead of traditional administrative boundaries. The use of catchment units better reflects the hydrological continuity of natural systems, allowing for a more realistic representation of the spatial evolution of drought within natural landscapes and reducing potential biases caused by inconsistencies in statistical scales. Therefore, although the base datasets and model outputs have certain limitations, we believe that the methodological design—especially the incorporation of catchment boundaries and bias correction—enhanced the spatial consistency and robustness of trend interpretation in this study.

Looking forward, further research on drought propagation mechanisms should incorporate high-resolution regional climate models, ground-based observational datasets, and information on human interventions such as reservoir operations, groundwater extraction, irrigation practices, and policy regulation. These additions would improve model applicability and explanatory power at regional scales. Meanwhile, greater emphasis should be placed on the integration and application of remote sensing data, with cross-validation using field measurements to achieve multi-source, joint characterization of drought propagation processes. Moreover, building an uncertainty assessment system that integrates multi-source data within the current framework would allow for enhanced comparison and validation of drought risk projections across different models, scenarios, and regions—thereby supporting more actionable drought early warning and adaptive management strategies.

Regarding bias correction methods, future studies could incorporate other advanced approaches commonly used for climate data calibration, such as Quantile Mapping and Cumulative Distribution Function transform (CDF-t). Moreover, multivariate bias correction methods (e.g., Multivariate Quantile Mapping) offer distinct advantages in capturing the coupled relationships among variables, making them particularly suitable for studies involving multi-variable interactions, such as drought propagation. Through comparative analysis and integration of multiple methods, the accuracy of calibration could be further improved, thereby enhancing the regional applicability and interpretability of model simulation results.

Regarding the calculation of drought propagation indices, although this study used the Drought Intensity Propagation Index (DIP) and Drought Duration Propagation Index (DDP), both of which were based on the temporal correspondence between standardized meteorological and hydrological indicators to provide a simple and practical framework for quantifying interregional drought propagation differences, we recognize that the current formulation may not fully account for the complex drivers of drought propagation. For instance, in heavily regulated basins, water resource policies, land use change, and irrigation practices may significantly influence both the pathways and impacts of drought propagation. In addition, limitations in the spatial resolution and temporal coverage of socio-economic and hydrological data may affect the accuracy of the propagation assessment. Future research could expand upon the current indices by incorporating multi-source, heterogeneous data to improve their adaptability and explanatory power in the context of multifactor drought propagation.

In terms of drought partitioning, this study focused on three key and representative drought partitions, systematically analyzing their evolution and trends under different climate scenarios to identify typical patterns and critical pathways of drought propagation on a global scale. However, we acknowledge that the current classification framework involves certain spatial simplifications and may not fully reflect the complex heterogeneity of natural conditions and anthropogenic influences across regions. Future studies should aim to develop higher-resolution drought partitioning methods by integrating data on land use change, water management, policy interventions, and socio-economic vulnerability. Such refined, context-specific classifications would enable deeper insights into the mechanisms of drought propagation and offer more targeted guidance for drought risk management.

5. Conclusions

This study primarily investigates the changes in the drought propagation process, specifically the changes in drought propagation partitions (H-dp, S-dp, and A-dp) under different Shared Socioeconomic Pathways (SSP1-2.6, SSP3-7.0, and SSP5-8.5), including the cases with and without human activities. The results show that, in all the scenarios, the proportion of S-dp is the largest globally, accounting for over 44 %, followed by A-dp and H-dp regions (both above 19 %). In the scenario without human activities, H-dp occupies the highest proportion, while A-dp occupies the smallest. From the SSP1-2.6 to the SSP5-8.5 scenario, the proportions of H-dp decreases gradually, while the proportions of A-dp and S-dp increases in future. Notably, the changes in South America are particularly significant, with nearly one-third of H-dp is disappearing, while the area of A-dp is doubling (under the SSP5-8.5 scenario). In the future, the areas of changes in drought partitions in the humid regions and Semi-Arid regions will account for the largest proportion in all the climate zones. Specifically, in the humid regions, the transition is from H-dp to S-dp, while in the Semi-Arid regions, it is from S-dp to A-dp. In the regions with better moisture conditions (such as Dry sub-humid regions and Humid regions), moderate human activities contribute to the improving regional drought conditions and promote the development from A-dp to S-dp (based on comparisons with and without human activities). However, overall, human activities are expected to drive drought partitions to an unfavorable direction (under the SSP5-8.5 scenario, approximately 2.4 % of regions exhibit a trend of unfavorable development). In particular, the changes in drought propagation patterns are most pronounced in the Great Plains of the United States, southern and central Europe, and around the Amazon Basin in South America. Reduced precipitation, increased evaporation, and enhanced land–atmosphere coupling are the main driving factors in these regions. This study further clarifies the changing trends in global drought conditions, providing important reference information for drought prediction and management in the context of climate change.

CRediT authorship contribution statement

Qiaoqiao Li: Writing – original draft, Validation, Software, Methodology, Data curation, Conceptualization. **Aizhong Ye:** Writing –

review & editing, Validation, Supervision, Funding acquisition, Conceptualization. **Reshmita Nath:** Writing – review & editing, Validation, Supervision. **Yuhang Zhang:** Writing – review & editing, Validation. **Junju Zhou:** Writing – review & editing, Validation.

Declaration of competing interest

The authors declare that they have no known competing financial interests or personal relationships that could have appeared to influence the work reported in this paper.

Acknowledgments

This study was supported by the National Key Research and Development Program of China (No. 2024YFF1306305), the Natural Science Foundation of China (No. 42171022), the BNU-FGS Global Environmental Change Program (No.2023-GC-ZYTS-06), and the China Scholarship Council (No.202306040129).

Appendix A. Supplementary data

Supplementary data to this article can be found online at https://doi.org/10.1016/j.ecolind.2025.113838.

Data availability

All data and software used in this study are openly available and can be accessed through the following sources: Precipitation data set: provided by ECMWF (Muñoz-Sabater et al., 2019) and ISIMIP 3b (Gosling et al., 2024). Soil moisture data set: provided by ECMWF (Muñoz-Sabater et al., 2019) and ISIMIP 3b (Gosling et al., 2024). Watershed boundaries: from the Hydro BASINS (Lehner and Grill, 2013). Climate classification data: produced by Antonio Trabucco and Robert Zomer (Trabucco and Zomer, 2009).

References

Ahmadi, B., Moradkhani, H., 2019. Revisiting hydrological drought propagation and recovery considering water quantity and quality. Hydrol. Process. 33 (10), 1492–1505.
Apurv, T., Sivapalan, M., Cai, X., 2017. Understanding the role of climate characteristics in drought propagation. Water Resour. Res. 53 (11), 9304–9329.
Bonan, G.B., 2008. Forests and climate change: forcings, feedbacks, and the climate benefits of forests. Science 320 (5882), 1444–1449.
Brubaker, K.L., Entekhabi, D., Eagleson, P.S., 1993. Estimation of continental precipitation recycling. J. Clim. 6 (6), 1077–1089.
Cheng, S., Guan, X., Huang, J., Ji, F., Guo, R., 2015. Long-term trend and variability of soil moisture over East Asia. J. Geophys. Res. Atmos. 120 (17), 8658–8670.
Costa, M.H., Foley, J.A., 2000. Combined effects of deforestation and doubled atmospheric CO2 concentrations on the climate of Amazonia. J. Clim. 13 (1), 18–34.
Dai, A., Lamb, P.J., Trenberth, K.E., Hulme, M., Jones, P.D., Xie, P., 2004. The recent Sahel drought is real. Int. J. Climatol. 24 (11), 1323–1331.
Davin, E.L., de Noblet-Ducoudr´e, N., 2010. Climatic impact of global-scale deforestation: radiative versus nonradiative processes. J. Clim.
Ding, Y.B., Xu, J.T., Wang, X.W., Cai, H., Zhou, Z., Sun, Y., Shi, H., 2021. Propagation of meteorological to hydrological drought for different climate regions in China. J. Environ. Manage. 283, 111980.
Dirmeyer, P.A., Jin, Y., Singh, B., Yan, X., 2013. Trends in land–atmosphere interactions from CMIP5 simulations. J. Hydrometeorol. 14 (3), 829–849.
Feng, S., Fu, Q., 2013. Expansion of global drylands under a warming climate. Atmos. Chem. Phys. 13 (19), 10081–10094.
Frieler, K., Lange, S., Piontek, F., Reyer, C.P.O., Schewe, J., Warszawski, L., Schaeffer, M., 2017. Assessing the impacts of 1.5°C global warming – simulation protocol of the Inter-Sectoral Impact Model Intercomparison Project (ISIMIP2b). Geosci. Model Dev. 10, 4321–4345.
Gosling, S. N., Müller Schmied, H., Burek, P., Guillaumot, L., Hanasaki, N., Kou-Giesbrecht, S., Otta, K., Sahu, R.-K., Satoh, Y., & Schewe, J. (2024). ISIMIP3b Simulation Data from the Global Water Sector (v1.1). *ISIMIP Repository*. https://doi.org/10.48364/ISIMIP.230418.1.
Gu, X., Zhang, Q., Li, J., Singh, V.P., Liu, J., Sun, P., Cheng, C., 2019. Attribution of global soil moisture drying to human activities: a quantitative viewpoint. Geophys. Res. Lett. 46 (5), 2573–2582.
Guan, D., Meng, J., Reiner, D.M., et al., 2018. Structural decline in China's CO2 emissions through transitions in industry and energy systems[J]. Nat. Geosci. 11 (8), 551–555.
Han, Z.M., Huang, S.Z., Huang, Q., Leng, G., Wang, H., Bai, Q., et al., 2019. Propagation dynamics from meteorological to groundwater drought and their possible influence factors. J. Hydrol. 578, 124104.
Heim Jr, R.R., 2002. A review of twentieth-century drought indices used in the United States. Bull. Am. Meteorol. Soc. 83 (8), 1149–1166.
Huang, S.Z., Huang, Q., Chang, J.X., et al., 2015. The response of agricultural drought to meteorological drought and the influencing factors: A case study in the Wei River Basin, China [J]. Agric. Water Manag. 159, 45–54.
Huang, J., Ji, M., Xie, Y., Wang, S., He, Y., Ran, J., 2016. Global semi-arid climate change over last 60 years. Clim. Dyn. 46, 1131–1150.
Huang, X., Yang, X., Wu, F., Zhang, J., 2025. Future propagation characteristics of meteorological drought to hydrological drought in the Yellow River basin. J. Hydrol. 649, 132443.
Husak, G.J., Michaelsen, J., Funk, C., 2007. Use of the gamma distribution to represent monthly rainfall in Africa for drought monitoring applications[J]. Int. J. Climatol: A Journal of the Royal Meteorological Society 27 (7), 935–944.
Jehanzaib, M., Shah, S.A., Kim, J.E., Kim, T.W., 2023. Exploring spatio-temporal variation of drought characteristics and propagation under climate change using multi-model ensemble projections. Nat. Hazards 115 (3), 2483–2503.
Konapala, G., Mishra, A.K., Wada, Y., Mann, M.E., 2020. Climate change will affect global water availability through compounding changes in seasonal precipitation and evaporation. Nat. Commun. 11 (1), 3044.
Kooperman, G.J., Chen, Y., Hoffman, F.M., et al., 2018. Forest response to rising CO2 drives zonally asymmetric rainfall change over tropical land. Nat. Clim. Chang. 8 (5), 434–440.
Lange, S., 2019. Trend-preserving bias adjustment and statistical downscaling with ISIMIP3BASD v1.0. Geosci. Model Dev. 12 (7), 3055–3070.
Lawrence, D., Vandecar, K., 2015. Effects of tropical deforestation on climate and agriculture. Nat. Clim. Chang. 5 (1), 27–36.
Lehner, B., Grill, G., 2013. Global river hydrography and network routing: baseline data and new approaches to study the world's large river systems. Hydrol. Process. 27 (15), 2171–2186. https://doi.org/10.1002/hyp.9740.
Li, Y., Brando, P.M., Morton, D.C., et al., 2022. Deforestation-induced climate change reduces carbon storage in remaining tropical forests[J]. Nat.Commun. 13 (1), 1964.
Li, X., Li, Y., Chen, A., et al., 2019. The impact of the 2009/2010 drought on vegetation growth and terrestrial carbon balance in Southwest China[J]. Agric. For. Meteorol. 269, 239–248.
Li, Q., Ye, A., Zhang, Y., Zhou, J., 2022a. The peer-to-peer type propagation from meteorological drought to soil moisture drought occurs in areas with strong land-atmosphere interaction. Water Resour. Res. 58 (9), e2022WR032846.
Li, Y., Brando, P.M., Morton, D.C., et al., 2022b. Deforestation-induced climate change reduces carbon storage in remaining tropical forests. Nat. Commun. 13 (1), 1964.
Li, Y., Zhao, M., Motesharrei, S., et al., 2015. Local cooling and warming effects of forests based on satellite observations[J]. Nat.Commun. 6 (1), 6603.
Liu, X., Li, C., Zhao, T., Han, L., 2020. Future changes of global potential evapotranspiration simulated from CMIP5 to CMIP6 models. Atmos. Oceanic Sci. Lett. 13 (6), 568–575.
Liu, Z., Wang, T., Yang, H., 2023. Overestimated global dryland expansion with substantial increases in vegetation productivity under climate warming. Environ. Res. Lett. 18 (5), 054024.
Ma, F., Yuan, X., Liu, X., 2023. Intensification of drought propagation over the Yangtze River basin under climate warming. Int. J. Climatol. 43 (12), 5640–5661.
Mahmood, R., Pielke Sr, R.A., Hubbard, K.G., et al., 2014. Land cover changes and their biogeophysical effects on climate. Int. J. Climatol. 34 (4), 929–953.
Mc Kee, T. B., Doesken, N. J., Kleist, J.1993. The relationship of drought frequency and duration to time scales[C]//Proceedings of the 8th Conference on Applied Climatology.Boston, MA: American Meteorological Society, 179–183.
Miralles, D.G., Teuling, A.J., Van Heerwaarden, C.C., et al., 2014. Mega-heatwave temperatures due to combined soil desiccation and atmospheric heat accumulation. Nat. Geosci. 7 (5), 345–349.
Mishra, A.K., Singh, V.P., 2010. A review of drought concepts. J. Hydrol. 391 (1–2), 202–216.
Mishra, A.K., Ines, A.V.M., Das, N.N., Prakash Khedun, C., Singh, V.P., Sivakumar, B., Hansen, J.W., 2015. Anatomy of a local-scale drought: Application of assimilated remote sensing products, crop model, and statistical methods to an agricultural drought study. J. Hydrol. 526, 15–29.
Mondal, S., Mishra, K.A., Leung, R., Cook, B., 2023. Global droughts connected by linkages between drought hubs. Nat. Commun. 14 (1), 144.
Muñoz-Sabater, J., Dutra, E., Agustí-Panareda, A., Albergel, C., Arduini, G., Balsamo, G., Boussetta, S., Choulga, M., Harrigan, S., Hersbach, H., Martens, B., 2021. ERA5-Land: A state-of-the-art global reanalysis dataset for land applications. Earth syst. sci. data 13 (9), 4349–4383.
Novick, K.A., Ficklin, D.L., Stoy, P.C., Williams, C.A., Bohrer, G., Oishi, A., et al., 2016. The increasing importance of atmospheric demand for ecosystem water and carbon fluxes. Nat. Clim. Chang. 6 (11), 1023–1027. https://doi.org/10.1038/nclimate3114.
Pokhrel, Y., Felfelani, F., Satoh, Y., Boulange, J., Burek, P., Gädeke, A., Wada, Y., 2021. Global terrestrial water storage and drought severity under climate change. Nat. Clim. Chang. 11 (3), 226–233.
Rousi, E., Kornhuber, K., Beobide-Arsuaga, G., et al., 2022. Accelerated western European heatwave trends linked to more-persistent double jets over Eurasia. Nat. Commun. 13 (1), 3851.
Sadhwani, K., Eldho, T.I., 2024. Assessing the effect of future climate change on drought characteristics and propagation from meteorological to hydrological droughts—A comparison of three indices. Water Resour. Manag. 38 (2), 441–462.

Schumacher, D.L., Keune, J., Dirmeyer, P., Miralles, D.G., 2022. Drought self-propagation in drylands due to land–atmosphere feedbacks. Nat. Geosci. 15 (4), 1–7. https://doi.org/10.1038/s41561-022-00912-7.
Seneviratne, S.I., Corti, T., Davin, E.L., et al., 2010. Investigating soil moisture–climate interactions in a changing climate: a review. Earth Sci. Rev. 99 (3–4), 125–161.
Seneviratne, S.I., Lüthi, D., Litschi, M., Schär, C., 2006. Land–atmosphere coupling and climate change in Europe. Nature 443 (7108), 205–209.
Smith, C., Baker, J.C.A., Spracklen, D.V., 2023. Tropical deforestation causes large reductions in observed precipitation. Nature 615 (7951), 270–275.
Sun, J., Zhang, Q., Xu, Y.J., Liu, X., Chen, L., Zhang, G., Wu, Y., 2025. Will drought evolution accelerate under future climate? J. Hydrol. 650, 132552.
Trabucco, A., Zomer, R., 2009. Global Aridity Index (Global-Aridity_ET0): a high-resolution global raster climate dataset from 1970 to 2000 (30 arc-seconds). J. Arid Environ. 73 (5), 636–644. https://doi.org/10.1016/j.jaridenv.2008.12.011.
Van Loon, A.F., 2013. On the Propagation of Drought.: how climate and Catchment Characteristics Influence Hydrological Drought Development and Recovery. Wageningen University and Research.
Vogel, M.M., Orth, R., Cheruy, F., et al., 2017. Regional amplification of projected changes in extreme temperatures strongly controlled by soil moisture-temperature feedbacks. Geophys. Res. Lett. 44 (3), 1511–1519.
Wu, G., Chen, J., Shi, X., Kim, J.S., Xia, J., Zhang, L., 2022. Impacts of global climate warming on meteorological and hydrological droughts and their propagations. Earth's Future 10 (3), e2021EF002542.
Xu, Y., Zhang, X., Hao, Z., et al., 2021. Characterization of agricultural drought propagation over China based on bivariate probabilistic quantification[J]. J. Hydrol. 598, 126194.
Yin, J., Gentine, P., Slater, L., Gu, L., Pokhrel, Y., Hanasaki, N., Schlenker, W., 2023. Future socio-ecosystem productivity threatened by compound drought–heatwave events. Nat. Sustainability 6 (3), 259–272.
Yuan, X., Wang, Y., Ji, P., Wu, P., Sheffield, J., Otkin, J.A., 2023. A global transition to flash droughts under climate change. Science 380 (6641), 187–191. https://doi.org/10.1126/science.abn6301.
Zhang, H., Henderson-Sellers, A., McGuffie, K., 1996. Impacts of tropical deforestation. Part I: Process analysis of local climatic change. J. Clim. 9 (7), 1497–1517.
Zhang, Q., Miao, C., Guo, X., Gou, J., Su, T., 2023. Human activities impact the propagation from meteorological to hydrological drought in the Yellow River Basin, China. J. Hydrol. 129752.
Zhang, S.W., Liu, Y., Cao, B.J., Li, S.Y., 2016. Soil moisture–precipitation coupling and trends in China, based on GLDAS and CMIP5 products. Climat. Environ. Res. 21 (2), 188–196.
Zhang, H., Ding, J., Wang, Y., et al., 2021. Investigation about the correlation and propagation among meteorological, agricultural and groundwater droughts over humid and arid/semi-arid basins in China[J]. Journal of hydrology 603, 127007.
Zhang, X., Hao, Z., Singh, V.P., Zhang, Y., Feng, S., Xu, Y., Hao, F., 2022. Drought propagation under global warming: Characteristics, approaches, processes, and controlling factors. Sci. Total Environ. 838, 156021.
Zheng, Y.Z., 2000. Overview of global natural disasters. Disaster Reduct. China 10 (1), 17–22. In Chinese.
Zhou, J.J., Li, Q.Q., Wang, L.Y., Lei, L., Huang, M., Xiang, J., et al., 2019. Impact of climate change and land-use on the propagation from meteorological drought to hydrological drought in the Eastern Qilian Mountains. Water 11 (8), 1602. https://doi.org/10.3390/w11081602.
Zhou, S., Yu, B., Zhang, Y., 2023. Global concurrent climate extremes exacerbated by anthropogenic climate change. Sci. Adv. 9 (10), eabo1638.
Zhu, Y., Liu, Y., Wang, W., et al., 2021. A global perspective on the probability of propagation of drought: From meteorological to soil moisture[J]. Journal of Hydrology 603, 126907.